Realtime measurement of phase partitioning of organic compounds using a Proton-Transfer-Reaction Time-of-Flight Mass Spectrometer coupled to a CHARON inlet

Yarong Peng[1,2], Hongli Wang[2,*], Yaqin Gao[2], Shengao Jing[2], Shuhui Zhu[2], Dandan Huang[2], Peizhi Hao[3], Shengrong Lou[2], Tiantao Cheng[4,5,*], Cheng Huang[2], Xuan Zhang[3,*]

[1] Department of Environmental Science and Engineering, Fudan University, Shanghai, 200438, China

[2] State Environmental Protection Key Laboratory of Formation and Prevention of Urban Air Pollution Complex, Shanghai Academy of Environmental Sciences, Shanghai, 200233, China

[3] School of Natural Sciences, University of California, Merced, 95343, USA

[4] Department of Atmospheric and Oceanic Sciences, Fudan University, Shanghai, 200438, China

[5] Big Data Institute for Carbon Emission and Environmental Pollution, Fudan University, Shanghai, 200438, China

Correspondence to: Hongli Wang (wanghl@saes.sh.cn), Tiantao Cheng (ttcheng@fudan.edu.cn), Xuan Zhang (xzhang87@ucmerced.edu)

Abstract. Understanding the gas-particle partitioning of semivolatile organic compounds (SVOCs) is of crucial importance in the accurate representation of the global budget of atmospheric organic aerosols. In this study, we quantified the gas- vs. particle-phase fractions of a large number of SVOCs in real time in an urban area of East China with the use of a CHemical Analysis of aeRosols ONline (CHARON) inlet coupled to a high resolution Proton Transfer Reaction Time-of-Flight Mass Spectrometer (PTR-ToF-MS). We demonstrated the use of the CHARON inlet for highly efficient collection of particulate SVOCs while maintaining the intact molecular structures of these compounds. The collected month-long dataset with hourly resolution allows us to examine the gas-particle partitioning of a variety of SVOCs under ambient conditions. By comparing the measurements with model predictions using the instantaneous equilibrium partitioning theory, we found that the dissociation of large parent molecules during the PTR ionization process likely introduces large uncertainties to the measured gas- vs. particle-phase fractions of less oxidized SVOCs, and therefore, caution should be taken when linking the molecular composition to the particle volatility when interpreting the PTR-ToF-MS data. Our analysis suggests that understanding the fragmentation mechanism of SVOCs and accounting for the neutral losses of small moieties during the molecular feature extraction from the raw PTR mass spectra could reduce, to a large extent, the uncertainties associated with the gas-particle partitioning measurement of SVOCs in the ambient atmosphere.

1. Introduction

Gas-particle partitioning of semivolatile organic compounds (SVOCs) is a critical process involved in the formation and evolution of atmospheric organic aerosols (OA). Traditionally,

gas-particle equilibrium partitioning of organic substances is assumed to be established instantaneously (Zhang and Seinfeld, 2013), this assumption is in question if particles are semi-solid or glassy (Shiraiwa et al., 2013). Most studies to date addressing the kinetic limitations in partitioning have used indirect and/or theoretical methods that are lack of chemical and molecular specificity (Mai et al., 2015; Shiraiwa and Seinfeld, 2012). Direct measurements of gas-particle partitioning of SVOCs are needed in order to develop accurate parameterizations for the organic aerosol formation in climate models.

The major challenge in the characterization of gas-particle partitioning of SVOCs lies in the realtime measurement of labile compounds while maintaining their intact molecular structures with minimal fragmentation (Zhang et al., 2016a; Zhang et al., 2016b; Zhang et al., 2019). In recent years, soft ionization techniques coupled to mass spectrometry have been widely used for the measurement of gas-phase SVOCs at the molecular level (Veres et al., 2008; Crounse et al., 2006; Heald and Kroll, 2020). Combined with thermal desorption methods, these techniques have also been deployed to measure organic compounds in both gas and particle phases nearly simultaneously (Krechmer et al., 2016). A notable example would be the use of the Filter Inlet for Gases and AEROsols coupled with the Chemical Ionization Mass Spectrometry (FIGAERO-CIMS) to quantify the gas-particle partitioning of a broad range of organic compounds in real time (Lopez-Hilfiker et al., 2014; Ye et al., 2021; Voliotis et al., 2021; Wang et al., 2020a; Lutz et al., 2019; Lee et al., 2018; Le Breton et al., 2018; Stark et al., 2017; Lopez-Hilfiker et al., 2016; Lopez-Hilfiker et al., 2015; Palm et al., 2020). A number of studies among those have reached a consensus that the thermograms method, i.e., using the calibrated thermal desorption profiles vs. temperature to derive the volatility, likely provides the best estimates of the actual phase distribution. In contrast, using the directly measured gas- and

64   particle-phase fractions of a given analyte will most likely introduce a significant positive or

65   negative bias to the volatility estimation due to the thermal decomposition of labile organic

66   compounds during the desorption process (Lopez-Hilfiker et al., 2015; Stark et al., 2017). Such

67   thermal decomposition (or ion fragmentation) artifacts, either positive or negative depending

68   on the molecular size, have been suggested to constitute the largest uncertainties in the

69   estimation of phase partitioning behaviors of SVOCs using the thermal desorption method at

70   ambient pressure (Thompson et al., 2016).

71   Along with the line of thermal desorption method development, an inlet designed for the

72   CHemical Analysis of aeRosols ONline (CHARON) has been developed and coupled to the

73   Proton Transfer Reaction Time-of-Flight Mass Spectrometer (PTR-ToF-MS) in recent years.

74   As CHARON-PTR-ToF-MS does not rely on any form of pre-concentration on surfaces, it

75   could provide online and direct measurements of organic compounds in both phases, compared

76   with traditional thermal desorption instruments which still need to address artifacts during the

77   particle collection and desorption processes. Another potential advantage of CHARON-PTR-

78   ToF-MS is that the chemical information of the collected particles can be studied qualitatively

79   and quantitatively over a chemical composition level even at sub-nanogram mass

80   concentrations per molecule owing to the well studied ion-molecule reaction chemistry in PTR-

81   ToF-MS (Piel et al., 2019). CHARON has shown promising potential in the realtime analysis

82   of the chemical composition and spatiotemporal distributions of aerosols with laboratory-,

83   ground-, and aircraft-based platforms (Piel et al., 2019; Tan et al., 2018; Gkatzelis et al., 2018a;

84   Gkatzelis et al., 2018b; Muller et al., 2017; Eichler et al., 2017; Eichler et al., 2015; Antonsen

85   et al., 2017; Leglise et al., 2019; Piel et al., 2021). As a relatively new technique, the use of

86   CHARON-PTR-ToF-MS to investigate the gas-particle partitioning of organic compounds is

87 still quite limited. Only one study by Gkatzelis et al. (2018b) deployed CHARON, together

88 with two other aerosol sampling inlets, to measure the OA formation and aging from

89 monoterpenes and real plant emissions in chamber experiments. Whether the CHARON inlet

90 can be applied to the study of gas-particle partitioning of organic compounds under the actual

91 atmospheric conditions remains to be validated.

92   In this study, we assess the applicability of the CHARON inlet to the time-resolved

93 collection of organic compounds in their native molecular state using laboratory tests with a

94 series of authentic standards. We further employ the CHARON inlet coupled to a high

95 resolution PTR-ToF-MS instrument to measure an array of gaseous and particulate SVOCs in

96 an urban area of East China. The obtained month-long hourly dataset allows us to examine the

97 gas-particle partitioning of SVOCs spanning a range of volatilities. By comparing the

98 measurements with model predictions using the instantaneous equilibrium partitioning theory,

99 we found that fragmentation during the PTR ionization process may introduce large

100 uncertainties to the measured gas- vs. particle-phase fractions of less oxidized SVOCs.

101 Understanding the dissociation patterns of parent molecules and accounting for the

102 fragmentation losses when extracting the molecular features from the raw PTR mass spectra

103 are needed to improve the measured accuracy of SVOCs partitioning between the gas and

104 particle phase.

105

106 **2.   Material and Methods**

107 **2.1. Sampling site**

108   The sampling site located in the campus of the Shanghai Academy of Environmental

109 Science (SAES) is representative of a typical urban setting surrounded by restaurants, shopping

110 malls, and residential and commercial buildings (Fig. S1). Two traffic-heavy streets in the area

111 (Caobao Road and Humin Highway) are located ~ 150 m and 450 m lateral distances to the east

112 of the sampling site. A few number of petrochemical and chemical industrial facilities are

113 located ~ 50 km to the south and southwest of the observation site, which likely bring certain

114 long-lived pollutants to the site at a typical wind speed of ~ 1 – 3 m/s. Major pollution sources

115 in the area include traffic, commercial and residential activities, and regional transport (Huang

116 et al., 2021; Peng et al., 2023). The sampling inlet of the PTR-ToF-MS instrument was installed

117 on the roof of an eight-story building ~ 24 m above the ground. A comprehensive measurement

118 of gas- and particle-phase compounds in the ambient air was performed from Oct 24 to Nov 22.

119 During the sampling period, the average temperature, relative humidity, and wind speed were

120 18.0 ± 3.0 °C, 61.0 ± 15.0%, and 1.8 ± 0.7 m/s, respectively. The prevailing wind direction in

121 this region was from the northwest and north during the polluted period (Fig. S2).

122 **2.2. CHARON-PTR-ToF-MS**

123 **2.2.1. Operation protocols**

124 A Proton Transfer Reaction Time-of-Flight Mass Spectrometer (PTR-ToF-MS) coupled to

125 a CHemical Analysis of aeRosols ONline (CHARON, Ionicon Analytik Inc, Innsbrunck,

126 Austria) inlet was employed to measure the gas- and particle-phase concentrations of a series

127 of SVOCs. The PTR-ToF-MS instrument used here is equipped with a radio frequency (RF)-

128 only quadrupole ion guide that transmits ions more efficiently (PTR-QiTOF, Ionicon Analytik

129 Inc). The operating parameters of the PTR-ToF-MS were held constant during the entire

130 measurement period. The drift tube pressure, temperature, and voltage were 2.9 mbar, 120 °C,

131 and 500 V, respectively. These conditions correspond to an E/N (E is the electric field, and N is

132 the number density of the gas molecules in the drift tube) value of ~ 100 Td (1 Td = 10^{-17} V

133   cm^2) and a reaction time of 120 μs. Note that the E/N value determines the collision energy of

134   ions in the reactor and therefore the degree of fragmentation and cluster formation. The

135   operating conditions were selected for the purpose of relatively low fragmentation intensities

136   (compared to 120 – 140 Td) and limited production of water clusters (compared to 60 – 80 Td).

137   Low E/N enhances the degree of water clustering, which complicates the analysis of analyte

138   ions due to a complex interplay between cluster formation ($RH^+(H_2O)_n$) and proton transfer

139   reactions (Holzinger et al., 2019). During the campaign, the sensitivity of the PTR-ToF-MS

140   was in the range of 300 – 1000 ncps ppb^{-1} and the mass resolution was maintained at ~ 5000

141   m/Δm. Mass spectra were collected at a time resolution of 10 s.

142   The CHARON inlet consists of 1) a gas-phase denuder (GPD) for stripping off gas-phase

143   analytes, 2) an aerodynamic lens (ADL) for particle collimation which is combined with an

144   inertial sampler for emanating the particle-enriched flow, and 3) a thermo-desorption unit (TDU)

145   for particle volatilization. The CHARON inlet functionality has been described in great detail

146   by Eichler et al. (2015). The inlet we used here had a particle enrichment factor of ~ 15, as

147   discussed shortly. The vaporizer (TDU) was operated at 140 °C and ~ 8 mbar absolute pressure.

148   Measurements of organic compounds in the gas and particle phase were conducted using a

149   parallel sampling system with two independent pumps, allowing for the selection of flow rates

150   specifically adjusted for each phase, resulting in the overall residence time of less than 2 s (Fig.

151   S3).

152   **2.2.2.   Sampling alternation between gas and particle phase**

153   Gas-phase compounds were measured by directly sampling the ambient air via a 2 m long

154   perfluoro-alkoxy (PFA) tube (1/4'' OD) capped with a polytetrafluoroethylene (PTFE) filter

155   (Mitex^{TM} PTFE membrane, 5 μm pore size, 47 mm diameter) to prevent the clogging of

particles in the PTR capillaries. The gas-phase inlet was independently connected to the PTR-ToF-MS instrument upstream of the drift tube via a pressure-controlled subsampling PEEK capillary (1/16" OD). Zero measurements were performed by overflowing catalytically (platinum at 370°C) purified air through the inlet. Ambient particles were sampled through a stainless steel tube (3/8" OD) with a flow rate of ~ 3 L min^{-1}, out of which a flow of ~ 500 ml min^{-1} was directed to the CHARON inlet. A PM$_{2.5}$ cyclone was installed in front of the sampling line to remove coarse particles (> 2.5 μm). The particle-phase background was measured by placing a High-Efficiency Particulate Air filter (HEPA, HEPA-CAP 7, GE Healthcare UK Limited, Buckinghamshire, UK) upstream of the CHARON inlet. Servo motor activated valves made of passivated stainless steel were used for switching between the two inlet configurations. During the campaign, CHARON-PTR-ToF-MS automatically switched between gas and particle phase every 15 min. Detailed setup is given in Fig. S3 in the Supporting Information.

The built-in PTR-manager software (Ionicon Analytik GmbH, Innsbruck, Austria) offers the possibility to program sequences by which the instrument switches between different settings. It takes ~ 1 min for gases and particles to re-equilibrate when switching between these two modes. Data generated during this transition period (~ 2 min) were not considered. Instrument background was measured for 15 min every 5h. The limits of detection (LoD) at 1 min resolution were in the range of 5.6 ± 2.9 ng m^{-3} for gases and 0.7 ± 0.5 ng m^{-3} for particles, respectively (Fig. S5). Concentrations of gaseous and particulate compounds shown here included the last 5 min of every gas/particle-phase working mode, in order to minimize the interferences carried over from the previous working mode by allowing for a sufficient amount of equilibration time in the inlet (Piel et al., 2021). In order to synchronize the gas- and particle-phase data to calculate gas-particle partitioning, the average hourly data were then used for

179   further analysis.

2.2.3.   Sensitivity and calibration

181   Weekly calibrations were performed using a multicomponent calibration gas standard

182   (Linde, USA) at five concentration levels from 0.5 to 10 ppb (Fig. S4a). The calibration mixture

183   includes methanol, acetonitrile, acetaldehyde, acrolein, acetone, isoprene, methyl vinyl ketone,

184   methyl ethyl ketone, 2-pentanone, toluene, styrene, p-xylene, 1,3,5-trimethylbenzene,

185   naphthalene and α-pinene. Here the sensitivity of PTR-ToF-MS is defined as the normalized

186   ion intensity of RH^+ (ncps) obtained at a mixing ratio of 1 ppb. For a given species (R), its

187   sensitivity (S, ncps ppb^{-1}) is a linear function of the rate constant of its reaction with H_3O^+ (k) :

$$S = \frac{\frac{I_{RH^+}}{I_{H_3O^+}} \times 10^6}{\frac{[R]}{N} \times 10^9} = k \times N \times 10^{-3} \times t \times \frac{T_{RH^+}}{T_{H_3O^+}} \times F_{RH^+} \tag{1}$$

$$\text{corrected } S = \frac{S}{\frac{T_{RH^+}}{T_{H_3O^+}} \times F_{RH^+}} = a \times k \tag{2}$$

190   where the signals of H_3O^+ ($I_{H_3O^+}$) and RH^+ ions (I_{RH^+}) measured by the mass analyzer (in cps)

191   can be related to the signals of H_3O^+ ($[H_3O^+]$) and RH^+ ($[RH^+]$) ions at the end of the drift tube,

192   using their respective transmission efficiencies ($T_{H_3O^+}$ and T_{RH^+}) from the drift tube to the

193   detector (De Gouw and Warneke, 2007). $[R]$ is the concentration of species R and N is the

194   number density of gas in the drift tube. The reaction time (t) is determined by the ion drift

195   velocity. F_{RH^+} represents the fraction of product ions detected as RH^+ ions ($0 \leq F_{RH^+} \leq 1$). For

196   non-fragmenting compounds, $F_{RH^+} = 1$. The measured sensitivity is further corrected by

197   accounting for fragmentation and transmission efficiency. The relative transmission efficiency

198   of ions was derived from laboratory experiments (Fig. S4a). a is the slope of the linear

199   regression of the corrected sensitivities on the proton-transfer-reaction rate coefficients (k), as

200 shown in Fig. S4b. Following the method by Sekimoto et al. (2017), the linear regression result

201 was used to determine the sensitivities of all uncalibrated species. The overall uncertainty was

202 less than 15% for compounds with standards and around 50% for those without standards.

203 Calculated sensitivity based on this method agrees well with measurements of authentic

204 standards (Fig. S4c).

2.2.4. Enrichment factor

206 The CHARON inlet was calibrated routinely with pure ammonium nitrate particles to

207 derive the enrichment factor as a function of the particle size following the procedures described

208 in Eichler et al. (2015). In addition, we used a selection of authentic standards (Table S1) to test

209 the effect of desorption temperature on the enrichment factor of labile compounds. Previous

210 studies with CHARON generally used a temperature of 140 °C to vaporize particles (Leglise et

211 al., 2019; Gkatzelis et al., 2018b; Tan et al., 2018). Herein, we tested the TDU temperature

212 ranging from 70 to 140°C. The selected chemical standards were individually dissolved in

213 distilled water (ethanol in the case of 2-Pentadecanone and 1-Pentadecanol) and nebulized by

214 an atomizer (TSI 3076, Shore-view, MN, USA) that was pressurized with ultrapure zero air.

215 The nebulizer outflow was diverted through two diffusion dryers to remove water vapor and an

216 activated charcoal denuder (NovaCarb F, Mast Carbon International Ltd., Guilford, UK) to

217 remove organic vapors. The resulting flow of polydisperse particles was then delivered into a

218 differential mobility analyzer (DMA, TSI 3080) for particle size selection. The transmitted

219 particles at a given size bin (300 nm for organics and 100 – 450 nm range for ammonium nitrate)

220 were introduced into the CHARON-PTR-ToF-MS analyzer and a condensation particle counter

221 (CPC, TSI 3775), respectively. Particle mass concentrations were calculated based on the CPC

222 number distribution measurements by assuming a shape factor of 0.8 for ammonium nitrate

223   particles and 1 for organic particles, respectively.

224   The particle enrichment factor (EF) of a given analyte i was calculated as the ratio of the

225   PTR-ToF-MS derived vs. CPC derived mass concentrations of analyte i at a given particle size

226   bin:

$$VMR_{(PTR)i} = \frac{I_i}{S_i} \tag{3}$$

$$VMR_{(CPC)i} = \rho_i \times V \times N_i \times V_m / Mw_i \tag{4}$$

$$EF = \frac{VMR_{(PTR)i}}{VMR_{(CPC)i}} \tag{5}$$

230   where I_i is the normalized signal of species i (ncps) by PTR-ToF-MS, S_i is the sensitivity

231   (ncps ppb^{-1}), VMR is the volume mixing ratio (ppb), ρ is the density of species i (g cm^{-3}),

232   V is the volume of a particle sphere (m^3), N_i is the number concentration of particles measured

233   by CPC (cm^{-3}), V_m is the molar volume of an ideal gas at 1 atm (22.4 L mol^{-1}), Mw_i is the

234   molecular weight (g mol^{-1}). As the calculated sensitivities of most organics in the absence of

235   authentic standards are subject to uncertainties (15% – 50%), we will herein use the

236   multiplication of EF and S_i to evaluate the combined effect of CHARON enrichment and

237   sensitivity on the measured concentrations of a given analyte i in the particle phase.

238   **2.2.5.   Data processing**

239   Data were analyzed using the Tofware package (v3.2.0, Tofwerk Inc), within the Igor Pro

240   software (v7.0, Wavemetrics). Using this package, time-dependent mass calibrations were

241   performed using four ions ($H_3^{18}O^+$, NO^+, $C_6H_5I^+$ and $C_6H_5I_2^+$), where $C_6H_5I^+$ and $C_6H_5I_2^+$ were

242   produced from the internal standard di-iodobenzene. The relative mass deviation was within 6

243   − 8 ppm across the mass spectra. Considering the humidity dependence of reagent ions (H_3O^+

244   and $H_3O^+(H_2O)$), the fitted product ion signals (RH^+) were normalized to a standard reagent ion

245 of 10^6 cps (counts per second). Elemental composition was determined based on the accurate

246 *m/z* (mass to charge ratio) and isotopic pattern analysis. A list of ~ 1600 ions was extracted,

247 including both gas- and particle-phase ions. Molecular formulas including only C, H, and O

248 atoms were assigned to the detected ions by the addition of one proton in cases where the

249 elemental composition analysis returned multiple options. About 85% of the signals were

250 elementally resolved by the $C_xH_yO_z$ formula in ambient air mass spectra. A small number of

251 nitrogen containing compounds, such as nitroaromatics, were also identified but not included

252 in the following analysis. Throughout of the context, we use the word "species" to refer to all

253 compounds with assigned molecular formula, which may include multiple isomers.

254 **2.3. Complementary measurements**

255   In addition to CHARON-PTR-ToF-MS, a Thermal desorption Aerosol Gas chromatograph

256 (TAG) was also employed to measure a series of particle-phase organic species. Details of the

257 TAG operation and data analysis protocols can be found in previous studies (He et al., 2020;

258 Wang et al., 2020b; Zhu et al., 2021). The elemental composition and mass concentration of

259 particles were measured by an Aerodyne high-resolution time-of-flight Aerosol Mass

260 Spectrometer (AMS), with details of operation and quality control protocols given by our recent

261 study (Huang et al., 2021). Volatile organic compounds (VOCs, $C_2 - C_{12}$) were analyzed by a

262 custom-built online gas chromatography system equipped with a mass spectrometer and a flame

263 ionization detector (GC-MS/FID). The performance of this system can be found in our previous

264 publications (Zhu et al., 2018; Wang et al., 2014). Meteorological parameters (ambient

265 temperature, wind speed, wind direction, and relative humidity) were collected by an automatic

266 weather station (Metone 590 series) mounted on the roof top of the campaign site.

2.4. Gas-particle partitioning measurements vs. modeling

The CHARON-PTR-ToF-MS measured gas- and particle-phase concentrations of a given species i can be used to calculate its particle-phase fraction ($F_{p,i}$).

$$P_i = \frac{\frac{I_{p,i} \times \left(\frac{m}{z}_i - 1\right)}{V_m \times S_i}}{EF} \tag{6}$$

$$G_i = \frac{I_{g,i} \times \left(\frac{m}{z}_i - 1\right)}{V_m \times S_i} \tag{7}$$

$$F_{p,i} = \frac{P_i}{P_i + G_i} \tag{8}$$

where P_i and G_i are the mass concentrations (ng m^{-3}) of species i in the particle and gas phase, respectively. $I_{p,i}$ and $I_{g,i}$ are the normalized signal (ncps) of the PTR-ToF-MS detected ion i in the particle and gas phase, respectively. V_m is taken as 22.4 L/mol. S_i is calculated or measured sensitivity (ncps ppb^{-1}), see details in Section 2.2.3. As structural isomers cannot be resolved in the mass spectra, the calculation here assumes that all isomers with the same molecular formula have the same chemical properties, i.e., saturation vapor pressures. Substitution of Equations (6) and (7) to Equation (8) yields the final expression of the particle-phase fraction of species i ($F_{p,i}$), which is a function of the observed PTR-MS raw signals of species i in the gas and particle phase (in total ion counts), as well as the particle enrichment factor (EF) of species i.

$$F_{p,i} = \frac{I_{p,i}/EF}{I_{p,i}/EF + I_{g,i}} \tag{9}$$

Gas-particle partitioning of a given analyte i was also modeled using the equilibrium partitioning theory (Pankow, 1994):

$$F_{p,i} = \frac{1}{1 + C_i^* / C_{OA}} \tag{10}$$

287
$$C_i^* = \frac{10^6 M w_i \zeta_i p_i}{RT} \tag{11}$$

288 where C_{OA} is the organic aerosol concentration measured by AMS (μg m^{-3}), C_i^* is the

289 saturation mass concentration (μg m^{-3}), Mw_i is the molecular weight (g mol^{-1}), ζ is the

290 activity coefficient (assumed as unity), p_i is the pure component liquid vapor pressure (Pa), R

291 is the universal gas constant (8.2 × 10^{-5} m^3 atm K^{-1} mol^{-1}), and T is the ambient temperature

292 (K). As detailed chemical information is lacking for all species detected by PTR-ToF-MS, here

293 we use the expression given by Donahue et al. (2011) to approximate the value of C_i^*:

294
$$\log_{10} C_i^* = \left(n_C^0 - n_C^i\right) b_C - n_O^i b_O - 2\frac{n_C^i n_O^i}{n_C^i + n_O^i} b_{CO} \tag{12}$$

295 where $n_C^0 = 25$, $b_C = 0.475$, $b_O = 2.3$, and $b_{CO} = -0.3$.

296

297 **2.5. Uncertainties in the measured and modeled gas-particle partitioning**

298 The uncertainty associated with the PTR-MS measured concentrations in both gas and

299 particle phases is less than 15% for compounds with chemical standards based on the optimally

300 fitted transmission efficiency curve. For those in the absence of standards, their PTR

301 sensitivities were calculated theoretically using Equations (1-2), and the uncertainty in the

302 calculation mainly arises from the estimation of polarizability and dipole moment of the target

303 molecule, which has been estimated to be within ~ 50% when only the elemental composition

304 of that molecule is given (Sekimoto et al., 2017). It is important to note, however, that the

305 uncertainty associated with the estimated PTR sensitivity has zero influence on the measured

306 particle-phase fraction of any given compound because the sensitivity term is essentially

307 canceled in the divisor function in Equation (9). The uncertainty associated with the particle

308 fraction of a given species i derived from the PTR-MS measurements arises predominantly

309 from the "*EF*" term. Since the uncertainty of the measured *EF* depends on the uncertainty of

310 $I_{p,i}$, we thus express the overall uncertainties of the measured gas-particle partitioning as:

311 $$Unc(F_{p,i})=\sqrt{Unc(\text{EF})^2+Unc(\text{I}_{g,i})^2} \tag{13}$$

312 with the calibration standards used in this study, the enrichment factor is calculated to be within

313 25% error ($Unc(\text{EF})$) (see detailed calculations listed in Table S2 and S3), including the effect

314 of wall loss inside the inlet tubing and the precision of the measurement. Huang et al. (2019)

315 has tested the uncertainty of wall loss ($Unc(\text{I}_{g,i})$) in this PTR-MS instrument as 28%. Therefore,

316 the overall uncertainty in the measured particle-phase fraction ($Unc(F_{p,i})$) was estimated as

317 38%.

318   The uncertainty associated with the modeled gas-particle partitioning arises primarily from

319 the uncertainty in the estimation of the saturation mass concentration (C_i^*) based on the method

320 developed by Donahue et al. (2011). In this method, the saturation mass concentration of

321 species *i* is a non-linear function of the numbers of carbon and oxygen atoms in that particular

322 species, see Equation (12). For each generic molecular formula, i.e., C_xH_y, C_xH_yO, $C_xH_yO_2$, and

323 $C_xH_yO_4$, Donahue et al. (2011) have used a total of 25, 48, 18, and 10 chemical standards with

324 known volatilities to validate the estimated saturation concentrations, and the estimated errors

325 were taken as 34%, 16%, 25%, and 54%, respectively (see Table S6). As the $C_xH_yO_3$ group was

326 not tested, we tentatively assumed the associated errors as the same as the $C_xH_yO_4$ group. The

327 extent to which these uncertainties may affect the difference between measurements and model

328 results was discussed in detail in the Supporting Information (Fig. S10).

329

3. Results and Discussion

3.1. Particle enrichment: effect of desorption temperature

Thermal desorption as a common procedure used in the chemical characterization of organic aerosols is often susceptible to fragmentation of non-refractory compounds. Due to the high temperature used to evaporate particles collected, labile and large molecules are inevitably subject to fragmentation, thereby introducing large uncertainties to the measured mass and composition of the particulate organic compounds (Lopez-Hilfiker et al., 2015; Yatavelli et al., 2012; Zhao et al., 2013). Thermal decomposition of oxidized organic compounds has been observed at vaporizer temperature as low as 200 °C, the lowest temperature required to vaporize OA as reported (Stark et al., 2017). While decreasing the vaporizer temperature is necessary to maintain the intact structure of labile molecules, low temperature (e.g., 85 °C), however, might fail to completely evaporate the collected particles into vapors, resulting in an underestimation of the collected OA mass (Inomata et al., 2014). Here we performed a series of sensitivity tests to identify the optimal vaporizer temperature in the CHARON inlet for the measurements of organic compounds in the particle phase.

Prior to the temperature sensitivity test, we have validated that the particle enrichment factor, also known as collection efficiency and defined as the ratio of the particle mass concentration upstream to downstream of the aerodynamic lens, does not depend on the particle size. As shown in Fig. 1a, the measured EF value for ammonium nitrate particles, detected as NO_2^+ produced from the nitric acid vapor, remains constant as ~ 15 in the $150-450$ nm particle size range. The lower values in the $100-150$ nm size range can be explained by the lower particle transmission efficiency in the gas phase denuder, e.g., 75% – 80% for 100 nm particles (Eichler et al., 2015). Also, particles below 150 nm are less efficiently concentrated in the

353 subsampling flow after the aerodynamic lens. Therefore, we used the monodisperse particles

354 generated from selected organic standards at 300 nm for the temperature sensitivity test.

355   A number of chemical standards that are representative of alcohols, carbonyls, and

356 carboxylic acids and with the vapor pressure ranging from 10^{-14} to 10^{-1} Pa at 25 °C (taken from

357 EPA EPI Suite (2012), see values given in Table S1) were used to generate organic aerosols,

358 which, upon size selection at 300 nm, were directed to the CHARON inlet. Particle evaporation

359 occurs downstream of the aerodynamic lens in the gas phase and on the tube and orifice surface

360 to which submicron particles rapidly diffuse at ~ 8 mbar operating pressure. The thermal

361 desorption unit was designed to ensure that ammonium sulfate particles (10^{-20} Pa) can be

362 completely evaporated (Piel et al., 2019; Eichler et al., 2015). As the desorption temperature

363 was varied from 70 °C to 140 °C, the intensities of all detected ions (including both parent and

364 fragment ions) for each organic standard analyzed were stable within 15%, as shown in Fig. 1b.

365 Also note that we did not observe any ions produced from decarboxylation and/or dehydration

366 during the particle evaporation process. This is because the relative low operation temperature

367 and the short heat exposure time could effectively limit any thermal dissociation of organic

368 molecules. This demonstrates that the parent molecule fragmentation, if any, does not occur

369 under the range of desorption temperature used in the CHARON inlet, but rather results from

370 the ionic dissociation process in the PTR ionization chamber, see more discussions in Section

371 3.3. We therefore used the sum total of intensities of all major ions detected as the PTR-ToF-

372 MS response to a given organic standard analyzed. Fig. 1c shows that the derived enrichment

373 factors stay constant for all compounds investigated (*Mw* ~ 160 – 230 g/mol). The relative

374 signals of all fragment ions were stable over the range of the desorption temperature as shown

375 in Fig. 2. This suggests that the desorption temperature used here, even as low as 70 °C, is

376 sufficient to evaporate SVOCs (volatility > 10^{-14} Pa at 25 °C), due to the low operating pressure

377 (~ 8 mbar) that significantly enhances the partitioning shift to the gas phase. One low volatility

378 compound, sucrose (*Mw* is 342 g/mol and vapor pressure is 4.69×10^{-14} Pa), has a slightly lower

379 enhancement factor compared with all the other organic standards tested. This is mainly due to

380 the intensive dehydration of the parent compound in the ionization chamber, and as a result,

381 only a few fragment ions were captured, resulting in a lower PTR response and thereby lower

382 *EF* value calculated from Equations (3-5). The *EF* values of sucrose also have much higher

383 standard deviations at all temperatures due to fragmentation (Table S3).
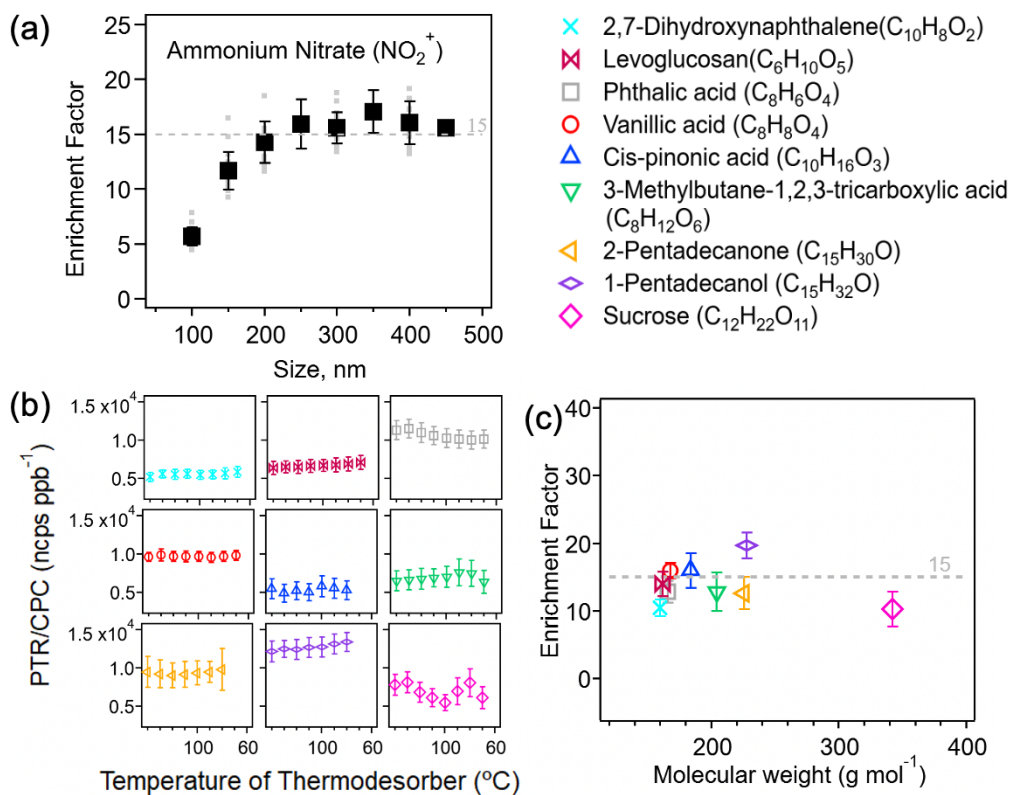
384

385 Figure 1. (a) Measured unitless enrichment factor (*EF*) of ammonium nitrate particles as a

function of particle size in the 100 – 450 nm range. Grey markers represent all replicating

measurements. The error bar denotes one standard deviation (1σ) of the average. (b) Ratios of

PTR-ToF-MS signals (including both parent and fragment ions) to CPC counts (±1σ) at 300

nm for all organic standards studied. (c) *EF* (±1σ) of selected organic standards based on the

calculated sensitivity.
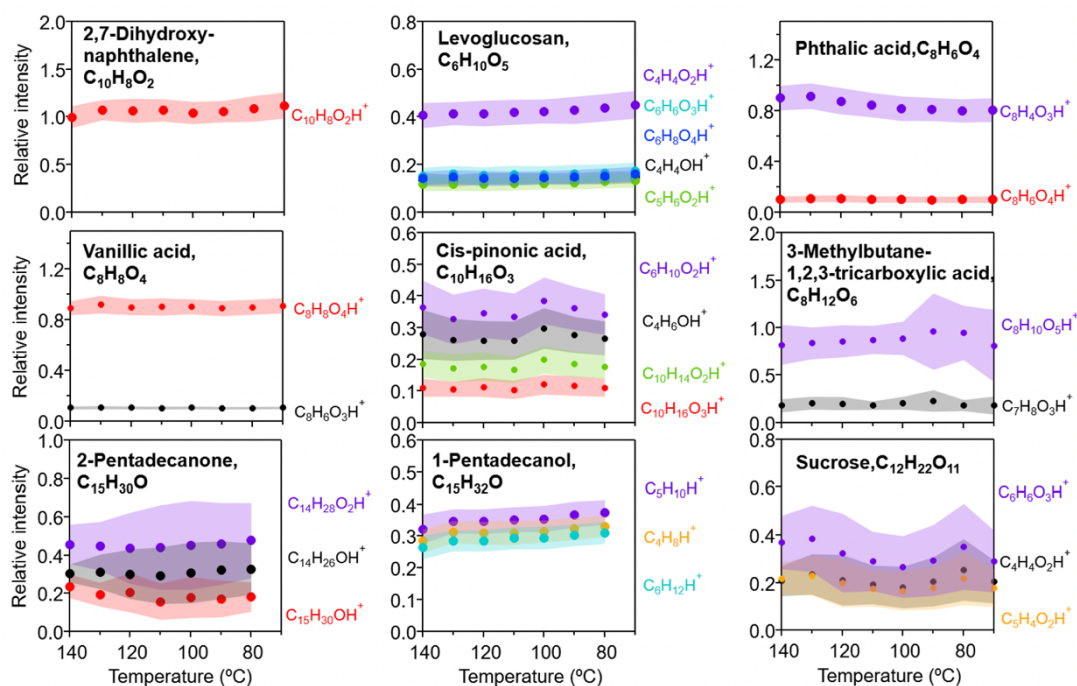
Figure 2. Ratios of CHARON-PTR-ToF-MS signals (ncps) to CPC measurements (ppb) of all

detected ions (including both parents and fragments) for a given pure organic standard tested

under different desorption temperatures (70 – 140 °C), normalized to the corresponding ratios

obtained at 140 °C. Ions with relative intensities less than 10% are excluded. Red markers

represent the parent peaks. Colored shades represent the relative standard deviations at different

398   temperatures (exact values are given in Table S4).

399   It has been recognized that species with one functional group follow certain fragmentation

400   patterns during the PTR ionization process (Pagonis et al., 2019; Francis et al., 2007; Spanel et

401   al., 1997; Tani et al., 2003; Spanel and Smith, 1997), such as dehydration of acids and alcohols.

402   The observed dissociation of carboxylic acid standards used in this study, e.g., phthalic acid

403   and 3-methylbutane-1,2,3-tricarboxylic acid, can be explained by this common fragmentation

404   pattern. The fragmentation mechanism of muti-functionalized species is rather complicated and

405   a number of fragments can be produced upon PTR ionization. Nevertheless, the identity and

406   abundance of fragments from a given muti-functionalized species have been found comparable

407   under the same PTR operation protocols (Leglise et al., 2019; Gkatzelis et al., 2018a). For

408   example, *cis*-pinonic acid yields the following fragments (main ions only and relative

409   abundance in parentheses): *m/z* 71.049 (~28%), 115.075 (~36%), 167.108 (~19%), and 185.117

410   (~11%), which is comparable with an earlier study (Leglise et al., 2019): *m/z* 71.049 (~27%),

411   115.075 (~33%), 167.108 (~26%), and 185.117 (~14%) at 100 Td settings.

412

413   **3.2. Molecular features of detected organic species**

414   A month-long field dataset of particle- and gas-phase organic species was collected at

415   hourly resolution using the CHARON-PTR-ToF-MS instrument. A comparison of PTR-ToF-

416   MS measurements with other techniques available on site was performed for both gas and

417   particle phases. For the gas phase, quantitative measurements of a suite of VOCs by GC-

418   MS/FID, including benzene, toluene, styrene, C_8 and C_9 aromatics, acrolein, and C_4, C_5, and C_6

419   ketones, agree well with corresponding PTR-ToF-MS measurements, as shown in Fig. S6. For

420   the particle phase, the time series of a group of $C_xH_yO_4$ species (including $C_4H_6O_4$, $C_5H_8O_4$,

421    $C_6H_{10}O_4$, and $C_8H_6O_4$) are in reasonable agreement with corresponding measurements taken by

422   TAG (r ~ 0.60 – 0.80), although the CHARON-PTR-ToF-MS measured total molecular mass

423   is generally lower than the TAG measurements by a factor of 2 to 6 (Fig. S7). This is likely

424   caused by the fragmentation (e.g., loss of H_2O, see Fig. S8) of the parent compounds during the

425   ionization process, as discussed in detail in Section 3.3. The time series of total OA mass

426   characterized by CHARON-PTR-ToF-MS also agree with the AMS measurements (r ~ 0.91,

427   Fig. S9). Previous studies have reported the particulate organics measured by PTR-MS with a

428   thermal desorption inlect account for 25% – 60% mass of the total organic aerosols measured

429   by AMS (Holzinger et al., 2013). Direct comparison of the total OA mass loading is not

430   applicable here since the CHARON-PTR-ToF-MS measurement only focused on compounds

431   with the mass to charge ratio below 300 Th. That the majority of ions detected by PTR are

432   present in the lower mass range is primarily due to the fragmentation of larger masses during

433   the ionization process, as discussed extensively in Section 3.3.
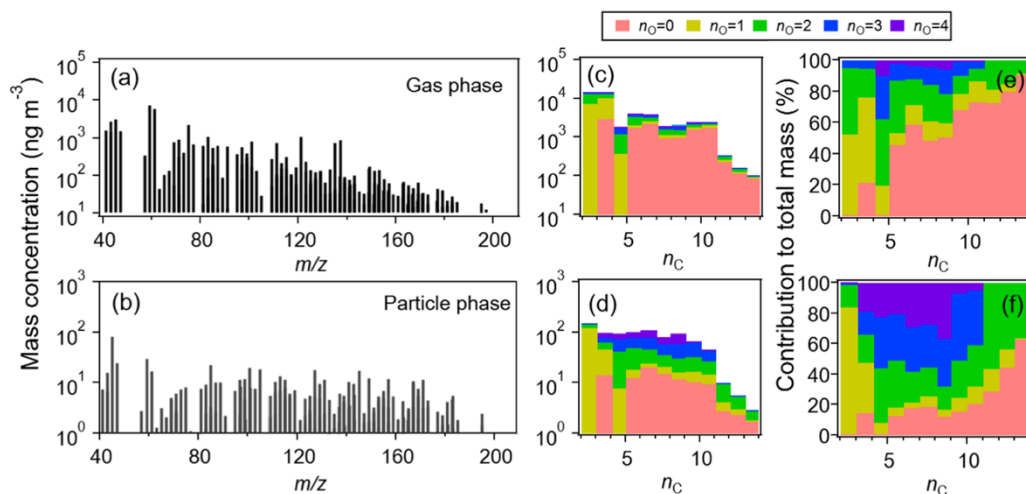
434

435   Figure 3. Background subtracted monthly-average PTR-ToF-MS mass spectra in the (a) gas

436   phase and (b) particle phase. Mass distributions of all identified species resolved by the carbon

437   and oxygen numbers (n_C and n_O) in the (c) gas phase and (d) particle phase, as well as their

438   relative contribution to the total organic mass in the (e) gas phase and (f) particle phase.

439

440   Fig. 3 (a-b) shows the PTR-ToF-MS spectra of dominant ions averaged over the entire

441   campaign in both gas and particle phases. The mass concentrations of individual ions are in the

442   range of 7.9 – 7179.3 ng m^{-3} in the gas phase and 0.6 – 82.7 ng m^{-3} in the particle phase. A total

443   of 152 species (with > 60% data points above the PTR-ToF-MS detection limits) are identified,

444   contributing to ~ 69% and ~ 44%, respectively, of the total organic mass measured in the gas

445   and particle phase. The molecular distribution characterized by the carbon and oxygen of these

446   species is given in Fig. 3 (c-d). The most abundant species are characterized by a generic

447   formula of C_xH_yO and $C_xH_yO_2$, resolving ~ 64% and ~ 46% in total of all identified species in

448   the gas and particle phase, respectively. Another dominant component in the gas phase is

449   hydrocarbon-like compounds (C_xH_y) (~ 27%), which contribute ~ 12% of the organic mass in

450   the particle phase. Species with higher oxygen numbers (> 2) contribute to a large fraction (~

451   42%) of the total particulate mass. These $C_xH_yO_{1-4}$ groups exhibit different diurnal cycles, as

452   shown in Fig. 4, reflecting their unique formation chemistry. The C_xH_y group peaks in the early

453   morning rush hour and likely originates from primary traffic emissions. On the contrary, both

454     $C_xH_yO_3$ and $C_xH_yO_4$ groups peak at noon, suggesting a strong secondary formation source. The

455   diurnal trends for C_xH_yO and $C_xH_yO_2$ groups are relatively flat during the day, likely indicative

456   of an intertwined primary emission and secondary formation processes.

457
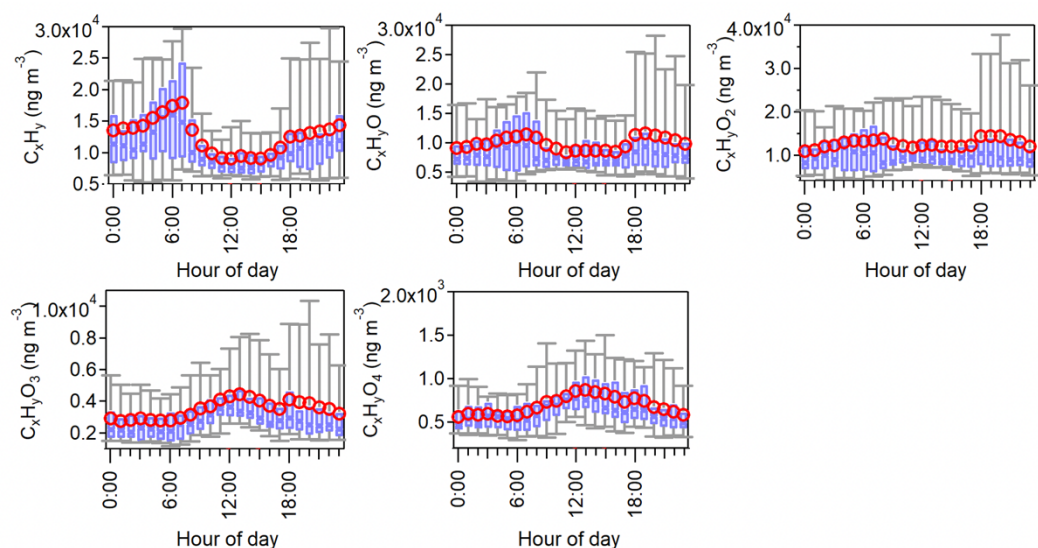
458

459 Figure 4. Diurnal variations of observed gas-phase species with a generic formula of $C_{2-13}H_{2-}$

460 $_{22}O_{0-4}$. Hourly average values (ng m^{-3}), together with 10th, 25th, 75th, and 90th percentiles, are

461 also plotted.

462

463 **3.3. Measured vs. modeled gas-particle partitioning**

464 Fig. 5 shows the calculated particle-phase fraction (F_p) of the identified 152 species using

465 the CHARON-PTR-ToF-MS measurements in both phases. It is important to note that an

466 authentic standard is not required for the calculation of F_p for any given species, because the

467 PTR sensitivity term is essentially canceled in the divisor function in Equations (6-8). Also

468 given in Fig. 5 is the simulated F_p of the derived molecular formulas of all species identified

469 using the equilibrium partitioning theory, see method described in Section 2.4. Interestingly,

470 for oxidized species such as $C_xH_yO_4$, their measured F_p agree reasonably with the simulations,

471 as shown in Fig. 5a. The $C_xH_yO_4$ group resides in the relatively higher mass range, and species

472   identified in this group are more likely actual compounds rather than fragments from larger

473   parent molecules. Even these species dessociate into lower mass ions during PTR ionization,

474   their calculated particle-phase fractions are unaffected by such fragmentation processes because

475   signals of parent ions decrease by the same extent upon fragmentation in both gas and particle

476   phases. As the oxygen number decreases, the measured F_p values tend to deviate from the

477   simulations by up to several orders of magnitude. Note that these less oxidized compounds (e.g.,

478   C_xH_y) are mostly small molecules and they are highly unlikely present in the condensed phase

479   as closed-shell monomers (Pankow and Asher, 2008; Holzinger et al., 2010). Instead, they are

480   more likely fragments produced from the decomposition of larger molecules, which no

481   surprisingly favor partitioning in the particle phase. The discrepancy in the measurement-model

482   comparison underscores the importance of understanding the fragmentation mechanism during

483   PTR ionization when extracting molecular features from the raw mass spectra.

484   Parent ion fragmentation has been widely observed in PTR-MS instruments (Pagonis et al.,

485   2019). Oxygenates exhibit trends in neutral losses of water or saturated alcohols. Here, we

486   apply a correction to the molecular formula of the 152 identified species by assuming that these

487   species are fragments produced from their parent precursors through the neutral losses of a

488   carboxyl group ($-CO_2$), a carbonyl group ($-CO$), a hydroxyl group ($-H_2O$), or an alcohol group

489   ($-C_2H_6O$). By applying this correction, the modeled F_p of a given species $C_xH_yO_z$ would actually

490   represent the particle-phase fraction of the its parent species $C_xH_yO_z \cdot CO_2$, $C_xH_yO_z \cdot CO$,

491     $C_xH_yO_z \cdot H_2O$, or $C_xH_yO_z \cdot C_2H_6O$. As shown in Fig. 5 (b-e), such a correction could significantly

492   increase the modeled F_p values by several orders of magnitude. The assumption of neutral

493   losses of CO_2 or C_2H_6O allows for much improved agreement between modeled vs. measured

494   F_p values for less oxidized species. This implies that these small and less oxidized species are

495 likely fragments resulting from the decomposition of larger parent precursors. As our particle

496 enrichment test (details given in Section 3.1) has confirmed that the thermal desorption

497 temperature employed for particle evaporation does not lead to any intensive fragmentation,

498 therefore the collision-induced dissociation during the proton transfer reaction process becomes

499 the predominant process that produces fragments (Lindinger et al., 1998; Gueneron et al., 2015;

500 Gkatzelis et al., 2018b). Although the electric field applied to the drift tube is considered low

501 to moderate compared with most previous PTR-MS measurements ($E/N \sim 100$ Td in this study

502 vs. $E/N \sim 120 - 140$ Td commonly found in PTR-MS measurements) (Pagonis et al., 2019),

503 parent ion fragmentation was still widely observed here and complicated the mass spectra

504 interpretation and molecular feature extraction. While some recent CHARON measurements

505 employed lower electric field in the drift tube ($E/N \sim 60$ Td) (Leglise et al., 2019; Gkatzelis et

506 al., 2018a; Piel et al., 2019), such conditions could promote the formation of water cluster ions,

507 which increase with humidity and reduce the PTR sensitivity, and therefore are not ideally

508 suitable for our field measurements. A compromise solution would be using a moderate electric

509 field in the drift tube (e.g., ~ 100 Td) and meanwhile applying appropriate molecular corrections

510 to all ions detected in the mass spectra by considering possible neutral losses of small moieties.

511 Since in this study only the information of molecular formula is derived from the PTR-MS

512 spectra, we thus provide the lower and upper bound of the gas-particle partitioning corrections

513 owing to neutral losses of H_2O and CO_2, respectively. In general, lower masses with higher

514 volatilities are subject to notable changes in the particle-phase fraction as a result of neutral

515 losses during the PTR ionization process, see detailed discussions in Text S1.

516

517
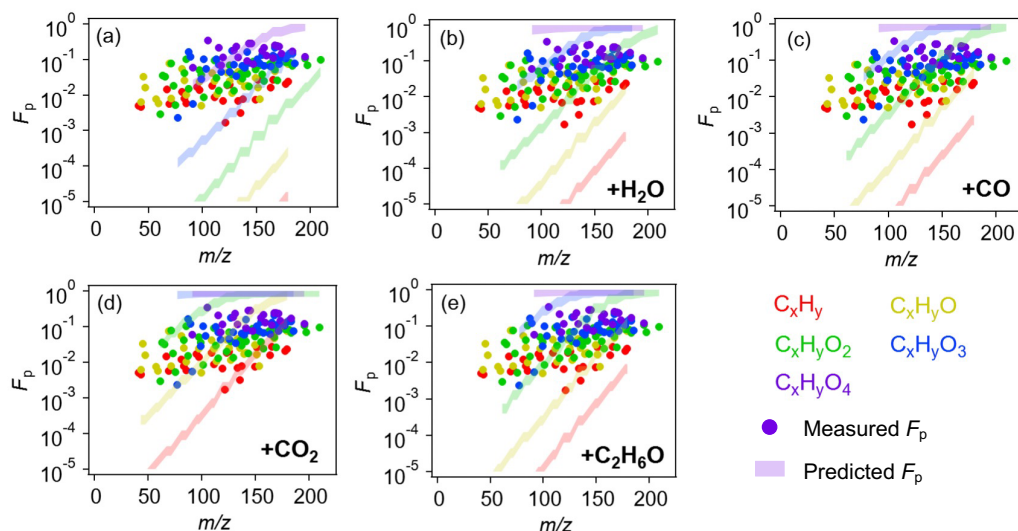
Figure 5. (a) Campaign average fraction of organic species in the particle phase (F_p) grouped by the oxygen number. Solid markers represent the calculated F_p based on the CHARON-PTR-ToF-MS measurements. Colored shades represent the predicted F_p of corresponding molecular formulas. (b-e) Measured vs. predicted F_p assuming the identified species are fragments of corresponding parent compounds through neutral losses of H_2O, CO, CO_2, and C_2H_6O, respectively (values are given in Table S5).

4. Conclusions

Recent studies have suggested that some of the model-measurement discrepancies in the representation of ambient organic aerosol budget might be due to the nonequilibrium gas/particle partitioning caused by kinetic limitations in the presence of glassy or semi-solid phase (Perraud et al., 2012; Mai et al., 2015; Shiraiwa et al., 2013). It is therefore necessary to validate whether the equilibrium partitioning theory could adequately describe the condensation of semivolatile organic vapors onto atmospheric aerosols under ambient

conditions, and the accurate measurement of these SVOCs in both gas and particle phases is the crucial prerequisite. In this study, we have employed the PTR-ToF-MS instrument coupled to a CHARON inlet, together with a suite of complementary measurements, to characterize the atmospheric partitioning behaviors of an array of SVOCs in an urban environment of East China. Prior to the application to the field measurements, we first performed a series of laboratory experiments to test whether the CHARON inlet is capable of sampling organic molecules (including alcohols, carbonyls, and carboxylic acids) in their native states. With the low pressure condition used in the CHARON inlet, a thermal desorption temperature less than 140 °C could adequately evaporate organic compounds with vapor pressure higher than 10^{-14} Pa while minimizing the thermal decomposition of labile functionalities. The auto-switch function between the gas and particle mode with one single PTR-ToF-MS instrument could monitor gaseous and particulate organic compounds in real time, thereby providing important information of their partitioning behaviors in the ambient atmosphere. Particle-phase fractions of a total of 152 organic species were derived from the CHARON-PTR-ToF-MS measurements and further compared with model predictions using the instantaneous equilibrium partitioning theory. While the model captured the particle-phase fraction of oxidized compounds (e.g., $C_xH_yO_{3-4}$), predictions of less oxidized compounds, notably the C_xH_y family, differ from the corresponding measurements by several orders of magnitude. Such a large discrepancy is very likely caused by the intensive fragmentation of the parent organic compounds during the PTR ionization process. Accounting for common fragmentation patterns in the simulations of gas-particle partitioning, for example, neutral losses of $-CO_2$, $-CO$, $-H_2O$, or $-C_2H_6O$, could largely improve the model-measurement agreement. Such corrections are very necessary towards an accurate measurement of both particle- and gas-phase SVOCs using the CHARON-PTR-ToF-

556 MS instrument. Our study suggests the crucial importance of optimizing operation conditions

557 and understanding the fragmentation mechanism in the particle collection, vaporization, and

558 ionization processes in understanding the gas-particle partitioning of organic compounds using

559 any thermal desorption based aerosol measurement method.

560

561 *Data availability.* The data shown in the paper are available upon request from the

562 corresponding author.

563 *Author Contributions.* YP carried out experiments and measurements and drafted the

564 manuscript. HW and XZ designed the experimental studies, supervised the laboratory work and

565 wrote the manuscript. YG and SJ supported the ambient measurements. SZ, DH, PH, and SL

566 supported the data analysis. TC and CH supervised the scientific work. All authors have given

567 approval to the final version of the manuscript.

568 *Competing interests.* The authors declare no competing financial interest.

569 *Acknowledgements.* This research has been supported by the National Natural Science

570 Foundation of China (No. 42175135, No. 42175179) and the Shanghai Science and Technology

571 Commission of the Shanghai Municipality (No. 20ZR1447800).

572

References

574 Antonsen, S., Bunkan, A. J. C., D'Anna, B., Eichler, P., Farren, N., Hallquist, M., Hamilton, J.
575 F., Kvarnliden, H., Mikoviny, T., Muller, M., Nielsen, C. J., Stenstrom, Y., Tan, W., Wisthaler,
576 A., and Zhu, L.: Atmospheric chemistry of tert-butylamine and AMP, in: Enrgy Proced, edited
577 by: Dixon, T., Laloui, L., and Twinning, S., Energy Procedia, Elsevier Science Bv, Amsterdam,
578 1026-1032, 10.1016/j.egypro.2017.03.1248, 2017.

579 Crounse, J. D., McKinney, K. A., Kwan, A. J., and Wennberg, P. O.: Measurement of gas-phase

580 hydroperoxides by chemical ionization mass spectrometry, Anal. Chem., 78, 6726-6732,
581 10.1021/ac0604235, 2006.

582 de Gouw, J. and Warneke, C.: Measurements of volatile organic compounds in the earths
583 atmosphere using proton-transfer-reaction mass spectrometry, Mass Spectrometry Reviews, 26,
584 223-257, 10.1002/mas.20119, 2007.

585 Donahue, N. M., Epstein, S. A., Pandis, S. N., and Robinson, A. L.: A two-dimensional
586 volatility basis set: 1. organic-aerosol mixing thermodynamics, Atmos. Chem. Phys., 11, 3303-
587 3318, 10.5194/acp-11-3303-2011, 2011.

588 Eichler, P., Muller, M., D'Anna, B., and Wisthaler, A.: A novel inlet system for online chemical
589 analysis of semi-volatile submicron particulate matter, Atmos. Meas. Tech., 8, 1353-1360,
590 10.5194/amt-8-1353-2015, 2015.

591 Eichler, P., Muller, M., Rohmann, C., Stengel, B., Orasche, J., Zimmermann, R., and Wisthaler,
592 A.: Lubricating Oil as a Major Constituent of Ship Exhaust Particles, Environ. Sci. Technol.
593 Lett., 4, 54-58, 10.1021/acs.estlett.6b00488, 2017.

594 EPA: Estimation Program Interface (EPI) Suite (v4.11), US [code], 2012.

595 Francis, G. J., Milligan, D. B., and McEwan, M. J.: Gas-Phase Reactions and Rearrangements
596 of Alkyl Esters with H3O+, NO+, and O2•+: A Selected Ion Flow Tube Study, J. Phys. Chem.
597 A, 111, 9670-9679, 10.1021/jp0731304, 2007.

598 Gkatzelis, G. I., Tillmann, R., Hohaus, T., Muller, M., Eichler, P., Xu, K. M., Schlag, P., Schmitt,
599 S. H., Wegener, R., Kaminski, M., Holzinger, R., Wisthaler, A., and Kiendler-Scharr, A.:
600 Comparison of three aerosol chemical characterization techniques utilizing PTR-ToF-MS: a
601 study on freshly formed and aged biogenic SOA, Atmos. Meas. Tech., 11, 1481-1500, 2018a.

602 Gkatzelis, G. I., Hohaus, T., Tillmann, R., Gensch, I., Muller, M., Eichler, P., Xu, K. M., Schlag,
603 P., Schmitt, S. H., Yu, Z. J., Wegener, R., Kaminski, M., Holzinger, R., Wisthaler, A., and
604 Kiendler-Scharr, A.: Gas-to-particle partitioning of major biogenic oxidation products: a study
605 on freshly formed and aged biogenic SOA, Atmos. Chem. Phys., 18, 12969-12989,
606 10.5194/acp-18-12969-2018, 2018b.

607 Gueneron, M., Erickson, M. H., VanderSchelden, G. S., and Jobson, B. T.: PTR-MS
608 fragmentation patterns of gasoline hydrocarbons, International Journal of Mass Spectrometry,

609 379, 97-109, 10.1016/j.ijms.2015.01.001, 2015.

610 He, X., Wang, Q., Huang, X. H. H., Huang, D. D., Zhou, M., Qiao, L., Zhu, S., Ma, Y.-g., Wang,
611 H.-l., Li, L., Huang, C., Xu, W., Worsnop, D. R., Goldstein, A. H., and Yu, J. Z.: Hourly
612 measurements of organic molecular markers in urban Shanghai, China: Observation of
613 enhanced formation of secondary organic aerosol during particulate matter episodic periods,
614 Atmos. Environ., 240, 10.1016/j.atmosenv.2020.117807, 2020.

615 Heald, C. L. and Kroll, J. H.: The fuel of atmospheric chemistry: Toward a complete description
616 of reactive organic carbon, Sci. Adv., 6, 10.1126/sciadv.aay8967, 2020.

617 Holzinger, R., Goldstein, A. H., Hayes, P. L., Jimenez, J. L., and Timkovsky, J.: Chemical
618 evolution of organic aerosol in Los Angeles during the CalNex 2010 study, Atmos. Chem. Phys.,
619 13, 10125-10141, 10.5194/acp-13-10125-2013, 2013.

620 Holzinger, R., Williams, J., Herrmann, F., Lelieveld, J., Donahue, N. M., and Rockmann, T.:
621 Aerosol analysis using a Thermal-Desorption Proton-Transfer-Reaction Mass Spectrometer
622 (TD-PTR-MS): a new approach to study processing of organic aerosols, Atmos. Chem. Phys.,
623 10, 2257-2267, 10.5194/acp-10-2257-2010, 2010.

624 Holzinger, R., Acton, W. J. F., Bloss, W. J., Breitenlechner, M., Crilley, L. R., Dusanter, S.,
625 Gonin, M., Gros, V., Keutsch, F. N., Kiendler-Scharr, A., Kramer, L. J., Krechmer, J. E.,
626 Languille, B., Locoge, N., Lopez-Hilfiker, F., Materić, D., Moreno, S., Nemitz, E., Quéléver,
627 L. L. J., Sarda Esteve, R., Sauvage, S., Schallhart, S., Sommariva, R., Tillmann, R., Wedel, S.,
628 Worton, D. R., Xu, K., and Zaytsev, A.: Validity and limitations of simple reaction kinetics to
629 calculate concentrations of organic compounds from ion counts in PTR-MS, Atmos. Meas.
630 Tech., 12, 6193-6208, 10.5194/amt-12-6193-2019, 2019.

631 Huang, D. D., Zhu, S., An, J., Wang, Q., Qiao, L., Zhou, M., He, X., Ma, Y., Sun, Y., Huang,
632 C., Yu, J. Z., and Zhang, Q.: Comparative Assessment of Cooking Emission Contributions to
633 Urban Organic Aerosol Using Online Molecular Tracers and Aerosol Mass Spectrometry
634 Measurements, Environ. Sci. Technol., 10.1021/acs.est.1c03280, 2021.

635 Huang, G., Liu, Y., Shao, M., Li, Y., Chen, Q., Zheng, Y., Wu, Z., Liu, Y., Wu, Y., Hu, M., Li,
636 X., Lu, S., Wang, C., Liu, J., Zheng, M., and Zhu, T.: Potentially Important Contribution of
637 Gas-Phase Oxidation of Naphthalene and Methylnaphthalene to Secondary Organic Aerosol
638 during Haze Events in Beijing, Environ. Sci. Technol., 53, 1235-1244, 10.1021/acs.est.8b04523,

639   2019.

640   Inomata, S., Sato, K., Hirokawa, J., Sakamoto, Y., Tanimoto, H., Okumura, M., Tohno, S., and
641   Imamura, T.: Analysis of secondary organic aerosols from ozonolysis of isoprene by proton
642   transfer   reaction   mass   spectrometry,   Atmos.   Environ.,   97,   397-405,
643   10.1016/j.atmosenv.2014.03.045, 2014.

644   Krechmer, J. E., Groessl, M., Zhang, X., Junninen, H., Massoli, P., Lambe, A. T., Kimmel, J.
645   R., Cubison, M. J., Graf, S., Lin, Y.-H., Budisulistiorini, S. H., Zhang, H., Surratt, J. D.,
646   Knochenmuss, R., Jayne, J. T., Worsnop, D. R., Jimenez, J.-L., and Canagaratna, M. R.: Ion
647   mobility spectrometry–mass spectrometry (IMS–MS) for on- and offline analysis of
648   atmospheric gas and aerosol species, Atmos. Meas. Tech., 9, 3245-3262, 10.5194/amt-9-3245-
649   2016, 2016.

650   Le Breton, M., Wang, Y. J., Hallquist, A. M., Pathak, R. K., Zheng, J., Yang, Y. D., Shang, D.
651   J., Glasius, M., Bannan, T. J., Liu, Q. Y., Chan, C. K., Percival, C. J., Zhu, W. F., Lou, S. R.,
652   Topping, D., Wang, Y. C., Yu, J. Z., Lu, K. D., Guo, S., Hu, M., and Hallquist, M.: Online gas-
653   and particle-phase measurements of organosulfates, organosulfonates and nitrooxy
654   organosulfates in Beijing utilizing a FIGAERO ToF-CIMS, Atmos. Chem. Phys., 18, 10355-
655   10371, 2018.

656   Lee, B. H., Lopez-Hilfiker, F. D., D'Ambro, E. L., Zhou, P., Boy, M., Petäjä, T., Hao, L.,
657   Virtanen, A., and Thornton, J. A.: Semi-volatile and highly oxygenated gaseous and particulate
658   organic compounds observed above a boreal forest canopy, Atmos. Chem. Phys., 18, 11547-
659   11562, 10.5194/acp-18-11547-2018, 2018.

660   Leglise, J., Muller, M., Piel, F., Otto, T., and Wisthaler, A.: Bulk Organic Aerosol Analysis by
661   Proton-Transfer-Reaction Mass Spectrometry: An Improved Methodology for the
662   Determination of Total Organic Mass, O:C and H:C Elemental Ratios, and the Average
663   Molecular Formula, Anal. Chem., 91, 12619-12624, 10.1021/acs.analchem.9b02949, 2019.

664   Lindinger, W., Hansel, A., and Jordan, A.: Proton-transfer-reaction mass spectrometry (PTR-
665   MS): on-line monitoring of volatile organic compounds at pptv levels, Chem. Soc. Rev., 27,
666   347-354, 10.1039/a827347z, 1998.

667   Lopez-Hilfiker, F. D., Mohr, C., Ehn, M., Rubach, F., Kleist, E., Wildt, J., Mentel, T. F., Lutz,
668   A., Hallquist, M., Worsnop, D., and Thornton, J. A.: A novel method for online analysis of gas

and particle composition: description and evaluation of a Filter Inlet for Gases and AEROsols (FIGAERO), Atmos. Meas. Tech., 7, 983-1001, 10.5194/amt-7-983-2014, 2014.

Lopez-Hilfiker, F. D., Mohr, C., Ehn, M., Rubach, F., Kleist, E., Wildt, J., Mentel, T. F., Carrasquillo, A. J., Daumit, K. E., Hunter, J. F., Kroll, J. H., Worsnop, D. R., and Thornton, J. A.: Phase partitioning and volatility of secondary organic aerosol components formed from α-pinene ozonolysis and OH oxidation: the importance of accretion products and other low volatility compounds, Atmos. Chem. Phys., 15, 7765-7776, 10.5194/acp-15-7765-2015, 2015.

Lopez-Hilfiker, F. D., Mohr, C., D'Ambro, E. L., Lutz, A., Riedel, T. P., Gaston, C. J., Iyer, S., Zhang, Z., Gold, A., Surratt, J. D., Lee, B. H., Kurten, T., Hu, W. W., Jimenez, J., Hallquist, M., and Thornton, J. A.: Molecular Composition and Volatility of Organic Aerosol in the Southeastern U.S.: Implications for IEPOX Derived SOA, Environ. Sci. Technol., 50, 2200-2209, 10.1021/acs.est.5b04769, 2016.

Lutz, A., Mohr, C., Le Breton, M., Lopez-Hilfiker, F. D., Priestley, M., Thornton, J. A., and Hallquist, M.: Gas to Particle Partitioning of Organic Acids in the Boreal Atmosphere, ACS Earth Space Chem., 3, 1279-1287, 10.1021/acsearthspacechem.9b00041, 2019.

Mai, H., Shiraiwa, M., Flagan, R. C., and Seinfeld, J. H.: Under What Conditions Can Equilibrium Gas-Particle Partitioning Be Expected to Hold in the Atmosphere?, Environ. Sci. Technol., 49, 11485-11491, 10.1021/acs.est.5b02587, 2015.

Muller, M., Eichler, P., D'Anna, B., Tan, W., and Wisthaler, A.: Direct Sampling and Analysis of Atmospheric Particulate Organic Matter by Proton-Transfer-Reaction Mass Spectrometry, Anal. Chem., 89, 10889-10897, 10.1021/acs.analchem.7b02582, 2017.

Pagonis, D., Sekimoto, K., and de Gouw, J.: A Library of Proton-Transfer Reactions of H3O+ Ions Used for Trace Gas Detection, Journal of the American Society for Mass Spectrometry, 30, 1330-1335, 10.1007/s13361-019-02209-3, 2019.

Palm, B. B., Peng, Q. Y., Fredrickson, C. D., Lee, B., Garofalo, L. A., Pothier, M. A., Kreidenweis, S. M., Farmer, D. K., Pokhrel, R. P., Shen, Y. J., Murphy, S. M., Permar, W., Hu, L., Campos, T. L., Hall, S. R., Ullmann, K., Zhang, X., Flocke, F., Fischer, E. V., and Thornton, J. A.: Quantification of organic aerosol and brown carbon evolution in fresh wildfire plumes, Proc Natl Acad Sci U S A, 117, 29469-29477, 10.1073/pnas.2012218117, 2020.

Pankow, J. F.: An absorption-model of the gas aerosol partitioning involved in the formation of

699   secondary organic aerosol, Atmos. Environ., 28, 189-193, 10.1016/1352-2310(94)90094-9,
700   1994.

701   Pankow, J. F. and Asher, W. E.: SIMPOL.1: a simple group contribution method for predicting
702   vapor pressures and enthalpies of vaporization of multifunctional organic compounds, Atmos.
703   Chem. Phys., 8, 2773-2796, 10.5194/acp-8-2773-2008, 2008.

704   Peng, Y., Wang, H., Wang, Q., Jing, S., An, J., Gao, Y., Huang, C., Yan, R., Dai, H., Cheng, T.,
705   Zhang, Q., Li, M., Hu, J., Shi, Z., Li, L., Lou, S., Tao, S., Hu, Q., Lu, J., and Chen, C.:
706   Observation-based sources evolution of non-methane hydrocarbons (NMHCs) in a megacity of
707   China, J. Environ. Sci., 124, 794-805, 10.1016/j.jes.2022.01.040, 2023.

708   Perraud, V., Bruns, E. A., Ezell, M. J., Johnson, S. N., Yu, Y., Alexander, M. L., Zelenyuk, A.,
709   Imre, D., Chang, W. L., Dabdub, D., Pankow, J. F., and Finlayson-Pitts, B. J.: Nonequilibrium
710   atmospheric secondary organic aerosol formation and growth, Proc Natl Acad Sci U S A, 109,
711   2836-2841, 10.1073/pnas.1119909109, 2012.

712   Piel, F., Muller, M., Mikoviny, T., Pusede, S. E., and Wisthaler, A.: Airborne measurements of
713   particulate organic matter by proton-transfer-reaction mass spectrometry (PTR-MS): a pilot
714   study, Atmos. Meas. Tech., 12, 5947-5958, 10.5194/amt-12-5947-2019, 2019.

715   Piel, F., Müller, M., Winkler, K., Skytte af Sätra, J., and Wisthaler, A.: Introducing the extended
716   volatility range proton-transfer-reaction mass spectrometer (EVR PTR-MS), Atmos. Meas.
717   Tech., 14, 1355-1363, 10.5194/amt-14-1355-2021, 2021.

718   Sekimoto, K., Li, S. M., Yuan, B., Koss, A., Coggon, M., Warneke, C., and de Gouw, J.:
719   Calculation of the sensitivity of proton-transfer-reaction mass spectrometry (PTR-MS) for
720   organic trace gases using molecular properties, International Journal of Mass Spectrometry, 421,
721   71-94, 10.1016/j.ijms.2017.04.006, 2017.

722   Shiraiwa, M. and Seinfeld, J. H.: Equilibration timescale of atmospheric secondary organic
723   aerosol partitioning, Geophysical Research Letters, 39, n/a-n/a, 10.1029/2012gl054008, 2012.

724   Shiraiwa, M., Zuend, A., Bertram, A. K., and Seinfeld, J. H.: Gas-particle partitioning of
725   atmospheric aerosols: interplay of physical state, non-ideal mixing and morphology, Phys.
726   Chem. Chem. Phys., 15, 11441-11453, 10.1039/c3cp51595h, 2013.

727   Spanel, P. and Smith, D.: SIFT studies of the reactions of H3O+, NO+ and O2+ with a series

728   of alcohols, Int. J. Mass Spectrom. Ion Processes, 167-168, 375-388,
729   https://doi.org/10.1016/S0168-1176(97)00085-2, 1997.

730   Spanel, P., Ji, Y. F., and Smith, D.: SIFT studies of the reactions of H3O+, NO+ and O-2(+)
731   with a series of aldehydes and ketones, International Journal of Mass Spectrometry, 165, 25-
732   37, 10.1016/s0168-1176(97)00166-3, 1997.

733   Stark, H., Yatavelli, R. L. N., Thompson, S. L., Kang, H., Krechmer, J. E., Kimmel, J. R., Palm,
734   B. B., Hu, W. W., Hayes, P. L., Day, D. A., Campuzano-Jost, P., Canagaratna, M. R., Jayne, J.
735   T., Worsnop, D. R., and Jimenez, J. L.: Impact of Thermal Decomposition on Thermal
736   Desorption Instruments: Advantage of Thermogram Analysis for Quantifying Volatility
737   Distributions of Organic Species, Environ. Sci. Technol., 51, 8491-8500,
738   10.1021/acs.est.7b00160, 2017.

739   Tan, W., Zhu, L., Mikoviny, T., Nielsen, C. J., Wisthaler, A., Eichler, P., Muller, M., D'Anna,
740   B., Farren, N. J., Hamilton, J. F., Pettersson, J. B. C., Hallquist, M., Antonsen, S., and Stenstrom,
741   Y.: Theoretical and Experimental Study on the Reaction of tert-Butylamine with OH Radicals
742   in the Atmosphere, J. Phys. Chem. A, 122, 4470-4480, 10.1021/acs.jpca.8b01862, 2018.

743   Tani, A., Hayward, S., and Hewitta, C. N.: Measurement of monoterpenes and related
744   compounds by proton transfer reaction-mass spectrometry (PTR-MS), International Journal of
745   Mass Spectrometry, 223, 561-578, 10.1016/s1387-3806(02)00880-1, 2003.

746   Thompson, S. L., Yatavelli, R. L. N., Stark, H., Kimmel, J. R., Krechmer, J. E., Day, D. A., Hu,
747   W., Isaacman-VanWertz, G., Yee, L., Goldstein, A. H., Khan, M. A. H., Holzinger, R., Kreisberg,
748   N., Lopez-Hilfiker, F. D., Mohr, C., Thornton, J. A., Jayne, J. T., Canagaratna, M., Worsnop, D.
749   R., and Jimenez, J. L.: Field intercomparison of the gas/particle partitioning of oxygenated
750   organics during the Southern Oxidant and Aerosol Study (SOAS) in 2013, Aerosol Sci. Technol.,
751   51, 30-56, 10.1080/02786826.2016.1254719, 2016.

752   Veres, P., Roberts, J. M., Warneke, C., Welsh-Bon, D., Zahniser, M., Herndon, S., Fall, R., and
753   de Gouw, J.: Development of negative-ion proton-transfer chemical-ionization mass
754   spectrometry (NI-PT-CIMS) for the measurement of gas-phase organic acids in the atmosphere,
755   International Journal of Mass Spectrometry, 274, 48-55, 10.1016/j.ijms.2008.04.032, 2008.

756   Voliotis, A., Wang, Y., Shao, Y., Du, M., Bannan, T. J., Percival, C. J., Pandis, S. N., Alfarra, M.
757   R., and McFiggans, G.: Exploring the composition and volatility of secondary organic aerosols

in mixed anthropogenic and biogenic precursor systems, Atmos. Chem. Phys., 21, 14251-14273, 10.5194/acp-21-14251-2021, 2021.

Wang, H. L., Lou, S. R., Huang, C., Qiao, L. P., Tang, X. B., Chen, C. H., Zeng, L. M., Wang, Q., Zhou, M., Lu, S. H., and Yu, X. N.: Source Profiles of Volatile Organic Compounds from Biomass Burning in Yangtze River Delta, China, Aerosol Air Qual. Res., 14, 818-828, 10.4209/aaqr.2013.05.0174, 2014.

Wang, M. Y., Chen, D. X., Xiao, M., Ye, Q., Stolzenburg, D., Hofbauer, V., Ye, P. L., Vogel, A. L., Mauldin, R. L., Amorim, A., Baccarini, A., Baumgartner, B., Brilke, S., Dada, L., Dias, A., Duplissy, J., Finkenzeller, H., Garmash, O., He, X. C., Hoyle, C. R., Kim, C., Kvashnin, A., Lehtipalo, K., Fischer, L., Molteni, U., Petaja, T., Pospisilova, V., Quelever, L. L. J., Rissanen, M., Simon, M., Tauber, C., Tome, A., Wagner, A. C., Weitz, L., Volkamer, R., Winkler, P. M., Kirkby, J., Worsnop, D. R., Kulmala, M., Baltensperger, U., Dommen, J., El Haddad, I., and Donahue, N. M.: Photo-oxidation of Aromatic Hydrocarbons Produces Low-Volatility Organic Compounds, Environ. Sci. Technol., 54, 7911-7921, 2020a.

Wang, Q. Q., He, X., Zhou, M., Huang, D. D., Qiao, L. P., Zhu, S. H., Ma, Y. G., Wang, H. L., Li, L., Huang, C., Huang, X. H. H., Xu, W., Worsnop, D., Goldstein, A. H., Guo, H., and Yu, J. Z.: Hourly Measurements of Organic Molecular Markers in Urban Shanghai, China: Primary Organic Aerosol Source Identification and Observation of Cooking Aerosol Aging, ACS Earth Space Chem., 4, 1670-1685, 2020b.

Yatavelli, R. L. N., Lopez-Hilfiker, F., Wargo, J. D., Kimmel, J. R., Cubison, M. J., Bertram, T. H., Jimenez, J. L., Gonin, M., Worsnop, D. R., and Thornton, J. A.: A Chemical Ionization High-Resolution Time-of-Flight Mass Spectrometer Coupled to a Micro Orifice Volatilization Impactor (MOVI-HRToF-CIMS) for Analysis of Gas and Particle-Phase Organic Species, Aerosol Sci. Technol., 46, 1313-1327, 2012.

Ye, C., Yuan, B., Lin, Y., Wang, Z., Hu, W., Li, T., Chen, W., Wu, C., Wang, C., Huang, S., Qi, J., Wang, B., Wang, C., Song, W., Wang, X., Zheng, E., Krechmer, J. E., Ye, P., Zhang, Z., Wang, X., Worsnop, D. R., and Shao, M.: Chemical characterization of oxygenated organic compounds in the gas phase and particle phase using iodide CIMS with FIGAERO in urban air, Atmos. Chem. Phys., 21, 8455-8478, 10.5194/acp-21-8455-2021, 2021.

Zhang, X. and Seinfeld, J. H.: A functional group oxidation model (FGOM) for SOA formation and aging, Atmos. Chem. Phys., 13, 5907-5926, 10.5194/acp-13-5907-2013, 2013.

789   Zhang, X., Dalleska, N. F., Huang, D. D., Bates, K. H., Sorooshian, A., Flagan, R. C., and
790   Seinfeld, J. H.: Time-resolved molecular characterization of organic aerosols by PILS plus
791   UPLC/ESI-Q-TOFMS, Atmos. Environ., 130, 180-189, 10.1016/j.atmosenv.2015.08.049,
792   2016a.

793   Zhang, X., Zhang, H. F., Xu, W., Wu, X. K., Tyndall, G. S., Orlando, J. J., Jayne, J. T., Worsnop,
794   D. R., and Canagaratna, M. R.: Molecular characterization of alkyl nitrates in atmospheric
795   aerosols by ion mobility mass spectrometry, Atmos. Meas. Tech., 12, 5535-5545, 10.5194/amt-
796   12-5535-2019, 2019.

797   Zhang, X., Krechmer, J. E., Groessl, M., Xu, W., Graf, S., Cubison, M., Jayne, J. T., Jimenez,
798   J. L., Worsnop, D. R., and Canagaratna, M. R.: A novel framework for molecular
799   characterization of atmospherically relevant organic compounds based on collision cross
800   section and mass-to-charge ratio, Atmos. Chem. Phys., 16, 12945-12959, 10.5194/acp-16-
801   12945-2016, 2016b.

802   Zhao, Y. L., Kreisberg, N. M., Worton, D. R., Isaacman, G., Weber, R. J., Liu, S., Day, D. A.,
803   Russell, L. M., Markovic, M. Z., VandenBoer, T. C., Murphy, J. G., Hering, S. V., and Goldstein,
804   A. H.: Insights into Secondary Organic Aerosol Formation Mechanisms from Measured
805   Gas/Particle Partitioning of Specific Organic Tracer Compounds, Environ. Sci. Technol., 47,
806   3781-3787, 2013.

807   Zhu, H., Wang, H., Jing, S., Wang, Y., Cheng, T., Tao, S., Lou, S., Qiao, L., Li, L., and Chen,
808   J.: Characteristics and sources of atmospheric volatile organic compounds (VOCs) along the
809   mid-lower Yangtze River in China, Atmos. Environ., 190, 232-240,
810   10.1016/j.atmosenv.2018.07.026, 2018.

811   Zhu, S., Wang, Q., Qiao, L., Zhou, M., Wang, S., Lou, S., Huang, D., Wang, Q., Jing, S., Wang,
812   H., Chen, C., Huang, C., and Yu, J. Z.: Tracer-based characterization of source variations of
813   PM2.5 and organic carbon in Shanghai influenced by the COVID-19 lockdown, Faraday
814   Discuss, 226, 112-137, 10.1039/d0fd00091d, 2021.

815